

Supplementary material to:
**Global sensitivity of aviation NO_x effects to the HNO₃-forming
channel of the HO₂ + NO reaction**

K. Gottschaldt, C. Voigt, P. Jöckel, M. Righi, R. Deckert and S. Dietmüller

January 15, 2013

Contents:	pages
1. Comparison of simulated versus observational profiles of selected trace gases	2 - 11
2. Additional information on chemical effects	12 - 16
3. Rate coefficient of $\text{CH}_4 + \text{OH} \rightarrow \text{CH}_3 + \text{OH}$	17 - 19
References	20

1 Comparison of simulated versus observational profiles of selected trace gases

In this section [HNO₃], [NO_x], [HO_x] and [O₃] profiles from simulations BA, DA and WA are compared to observational profiles of Emmons et al. (2000). The observational profile data are composites for different regions and campaigns. For this study we only selected data from near the year 2001, as listed in Table S1. The simulation data were sampled according to the observational region and time of year, but not at the exact location and time of the individual measurements that entered the observational composite data. Mean values were calculated from all model output steps in the given time range. Furthermore the observational profiles have been mostly compiled from different years than the simulation year 2001. The comparison is considered a climatological one. However, each simulation profile and each observational profile is based just on a few of days of data from a single year. Thus this comparison may only give an overall idea if the order of magnitude of the above trace gas mixing ratios is realistic in the simulations.

The observational data of Emmons et al. (2000) are limited to the altitude range below 11 km (Fig. S1). Thus differences between [HNO₃] profiles from simulations BA, DA and WA are generally small. Some model data are lower than the corresponding observations, some are higher. At least the extreme values do always overlap. HNO₃ is subject to scavenging, which strongly depends on local events like convection and rain. Individual scavenging events differ between model and observations, and may print through due to the short sampling periods. Furthermore, the heterogeneous reaction $\text{N}_2\text{O}_5 + \text{H}_2\text{O} \rightarrow 2\text{HNO}_3$ is calculated on all aerosol surfaces, throughout the atmosphere. However, in the troposphere N₂O₅ is rather converted into aqueous-phase NO₃⁻, but not released as gaseous HNO₃ (Jöckel et al., 2010). On the other hand, NO₃⁻ is potentially interpreted as HNO₃ in measurements (Keene et al., 1998). Since HNO₃_tot in Fig. 1 and in Fig. S1 contains only gaseous HNO₃ and NAT, errors concerning NO₃⁻ may partially compensate. Considering the above uncertainties, the model data match the [HNO₃] observations well.

[NO_x] observations are generally well reproduced by all simulations (Fig. S2). Measured and simulated values do always overlap, standard deviations do mostly. Some measurements are in better agreement with BA, others with DA or WA.

Standard deviations of simulated ozone mixing ratios overlap with almost all measurements (Fig. S3). Ozone observations are very well reproduced, and there is no clear bias in any of the simulations.

The significant impact of OH mixing ratios on [CO] is reflected in Fig. 4. The HNO₃-forming channel of HO₂ + NO (Reaction R2) shifts profiles of simulated [CO] from lower to higher values. CO mixing ratios are mostly lower than the observations for BA, but agree better for WA.

All three simulations (BA, DA, WA) match the observations well. Neither the chemical regime without the HNO₃-forming channel of HO₂ + NO, nor the two regimes with it can be ruled out according to this analysis.

Table S1. Campaign composite profile data (Emmons et al., 2000) used for the comparison to simulations BA, DA and WA in Fig. S1 – S4. The simulations were sampled for the same date ranges and region bounds as listed in this table. However, the simulation year characterised by synoptic dynamics and emissions was always 2001.

Campaign composite	Time range	year	lon _{min}	lon _{max}	lat _{min}	lat _{max}
PEM-Tropics-A_DC8 , Fiji	15.08.-15.10.	1996	170	-170	-30	-10
PEM-Tropics-A_DC8, Easter-Is.	15.08.-15.10.	1996	-120	-100	-40	-20
PEM-Tropics-A_DC8, Tahiti	15.08.-15.10.	1996	-160	-130	10	0
PEM-Tropics-A_DC8, X-mas-Is.	15.08.-15.10.	1996	-160	-140	0	10
TOPSE-Apr_C130, Boulder	02.04.-30.04.	2000	-110	-90	37	47
TOPSE-Apr_C130, Churchill	02.04.-30.04.	2000	-110	-80	47	65
TOPSE-Apr_C130, Thule	02.04.-30.04.	2000	-110	-60	65	90
TOPSE-Feb_C130, Boulder	04.02.-27.02.	2000	-110	-90	37	47
TOPSE-Feb_C130, Churchill	04.02.-27.02.	2000	-110	-80	47	65
TOPSE-Feb_C130, Thule	04.02.-27.02.	2000	-110	-60	65	90
TOPSE-Mar_C130, Boulder	05.03.-26.03.	2000	-110	-90	37	47
TOPSE-Mar_C130, Churchill	05.03.-26.03.	2000	-110	-80	47	65
TOPSE-Mar_C130, Thule	05.03.-26.03.	2000	-110	-60	65	90
TOPSE-May_C130, Boulder	15.05-23.05.	2000	-110	-90	37	47
TOPSE-May_C130, Churchill	15.05-23.05.	2000	-110	-80	47	65
TOPSE-May_C130, Thule	15.05-23.05.	2000	-110	-60	65	90
TRACE-P_DC8, China	24.02.-10.04.	2001	110	130	10	30
TRACE-P_DC8, Guam	24.02.-10.04.	2001	140	150	10	20
TRACE-P_DC8, Hawaii	24.02.-10.04.	2001	-170	-150	10	30
TRACE-P_DC8, Japan	24.02.-10.04.	2001	130	150	20	40

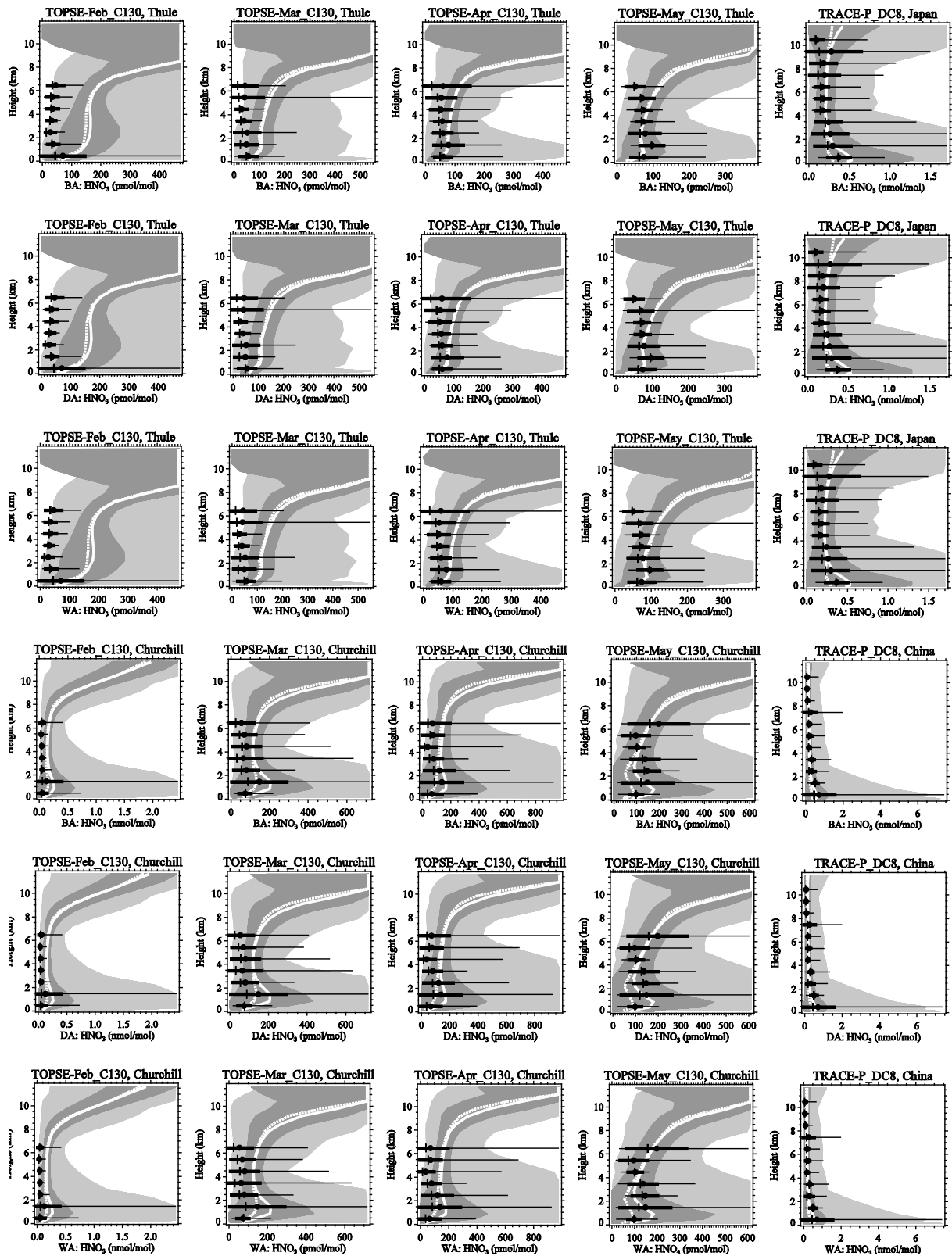


Figure S1a. Comparison of HNO_3 mixing ratio profiles as listed in Table S1. Black represents observational data: dot = mean, cross = median, thick error bar = standard deviation, thin error bar = range of values. Grey shading and white curves refer to simulations: solid line = mean, dotted line = median, dark grey = standard deviation, light grey = range of values (full range not always shown).

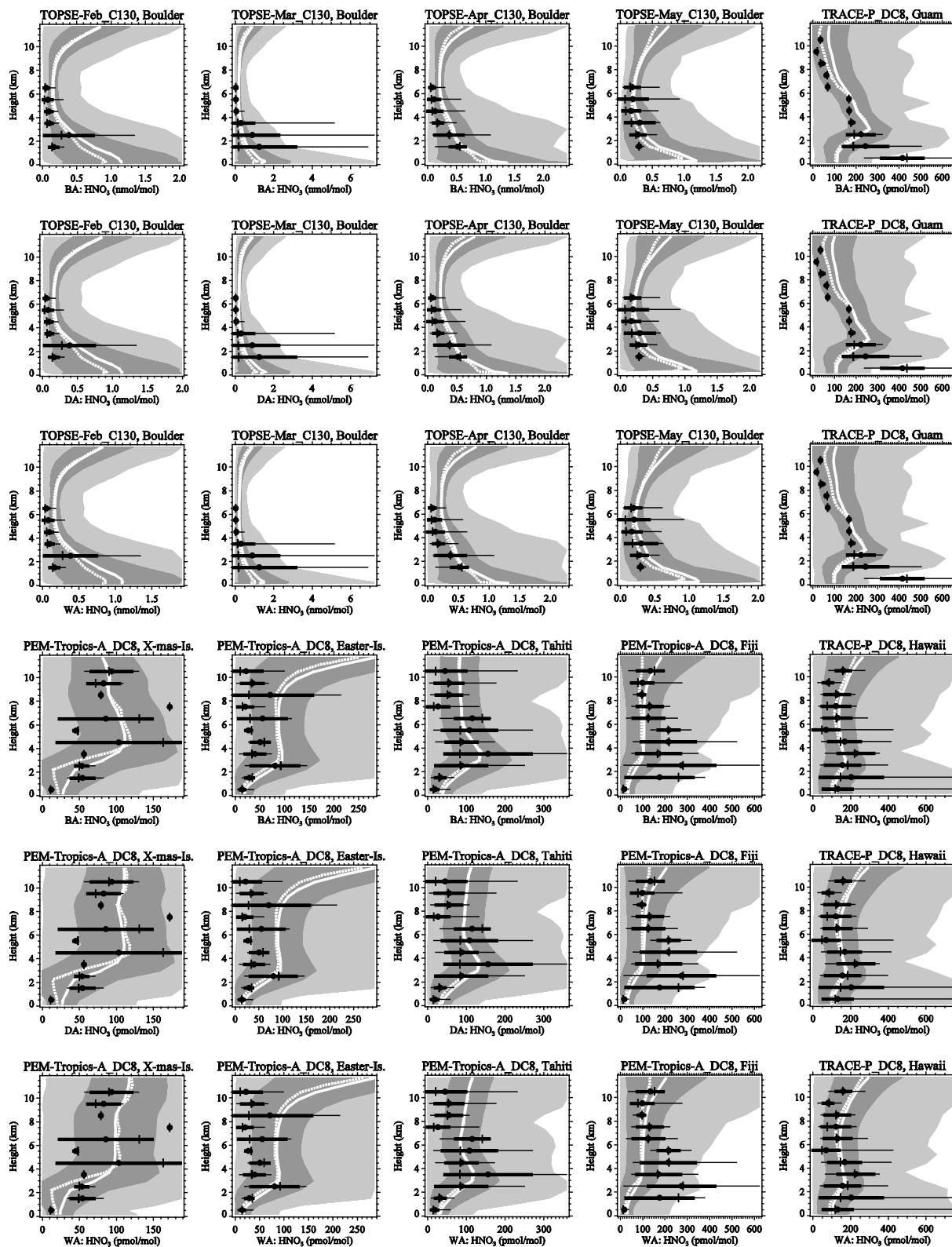


Figure S1b. Continued from Fig. S1a.

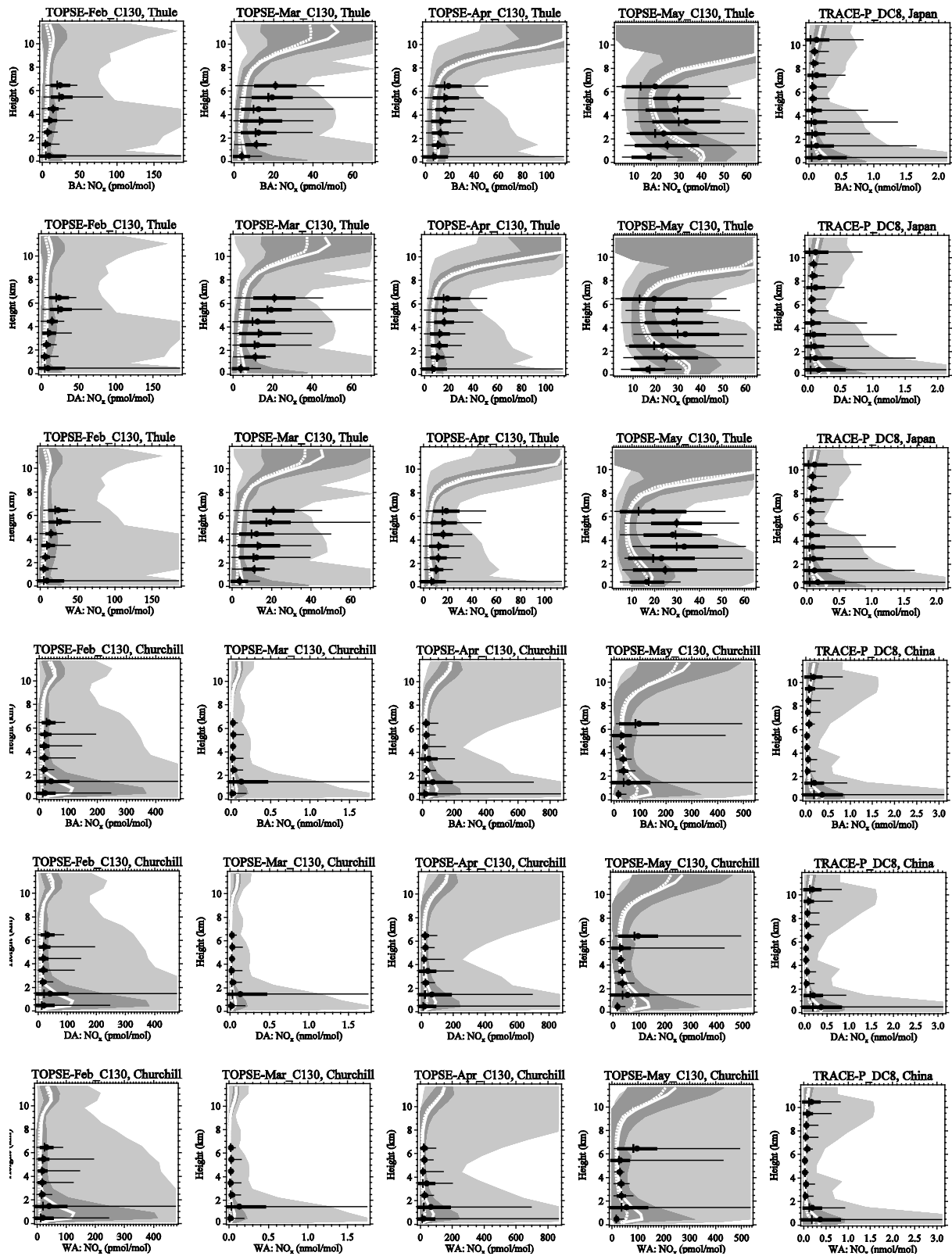


Figure S2a. As Fig. S1a, but for NO_x.

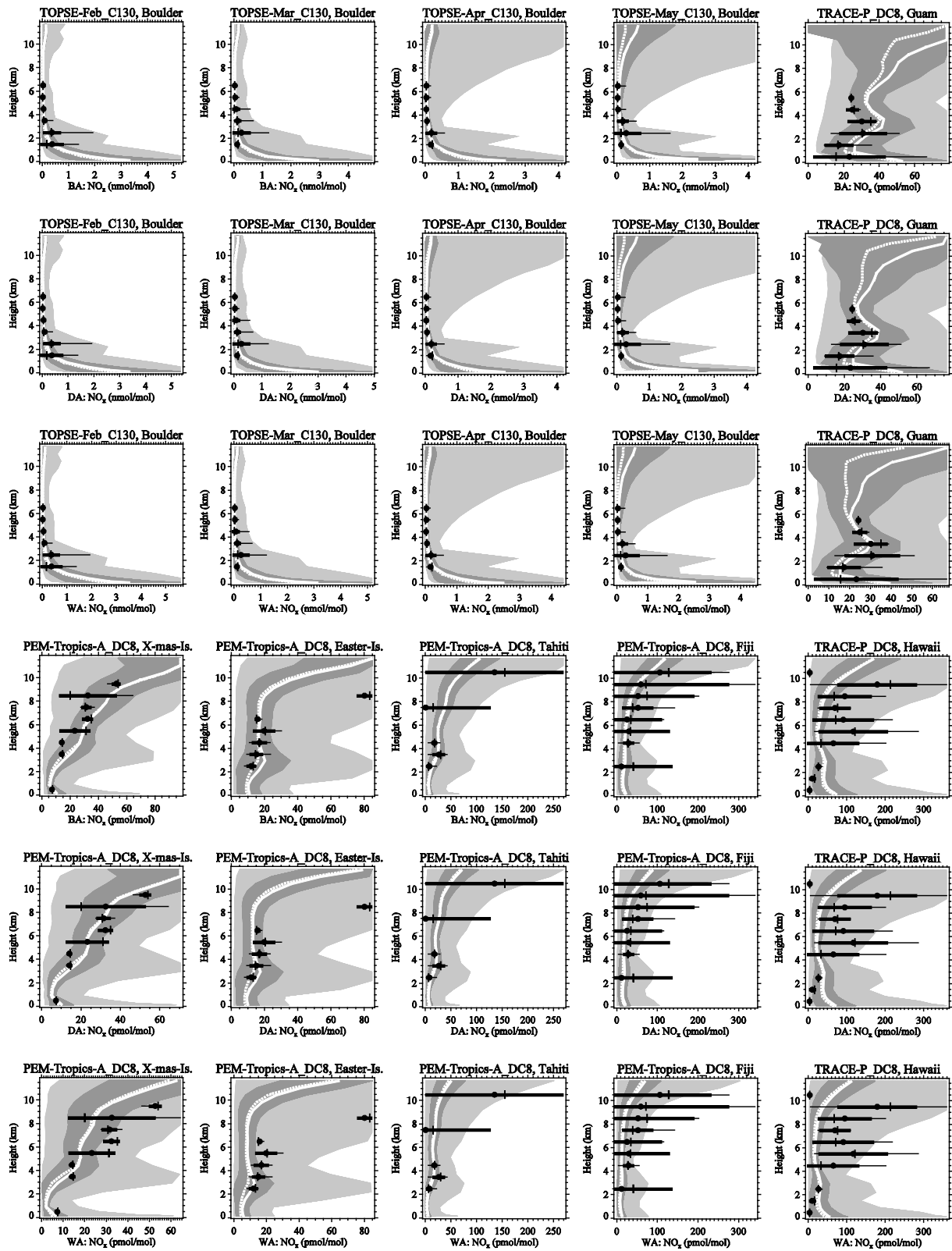


Figure S2b. Continued from Fig. S2a.

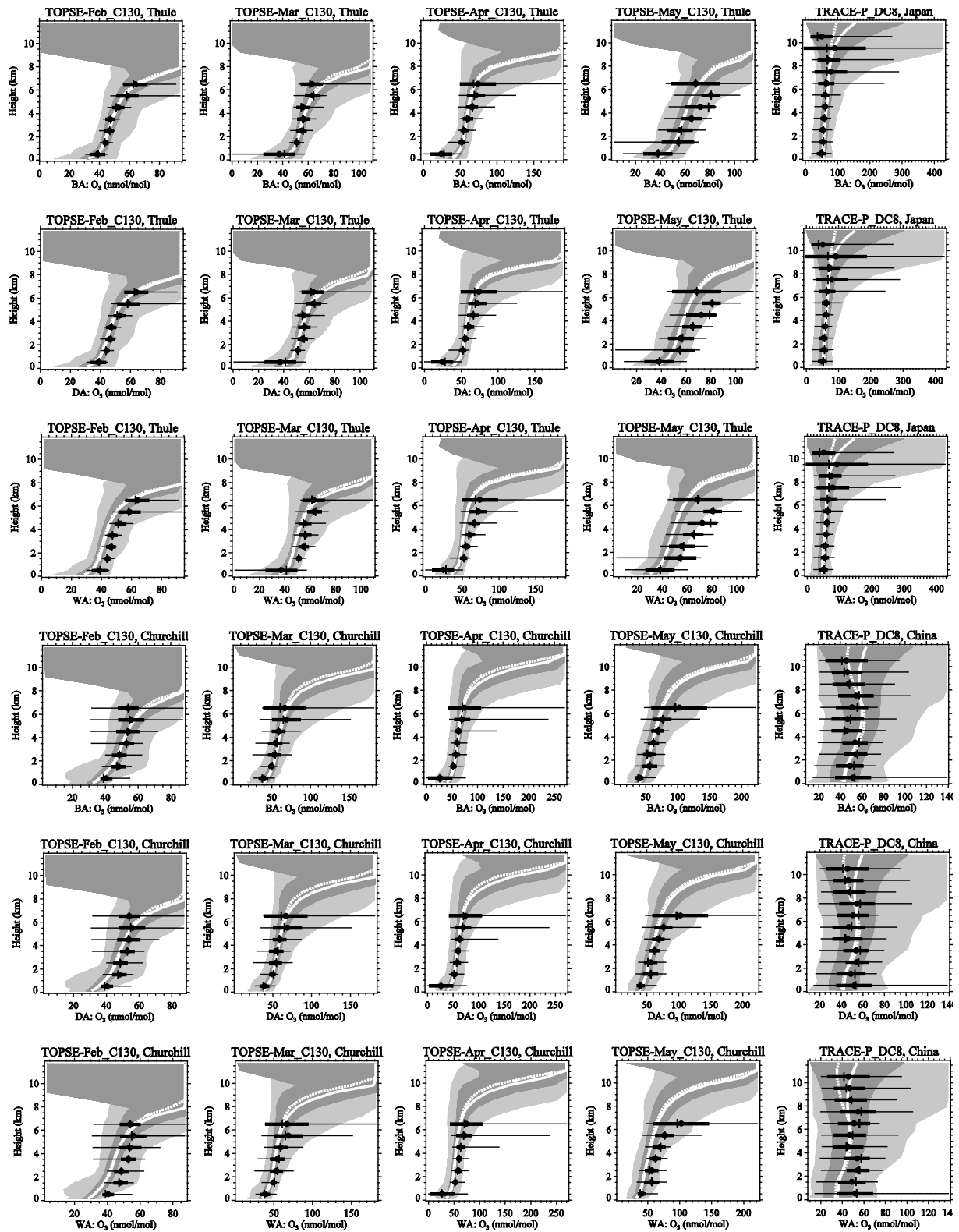


Figure S3a. As Fig. S1a, but for O_3 .

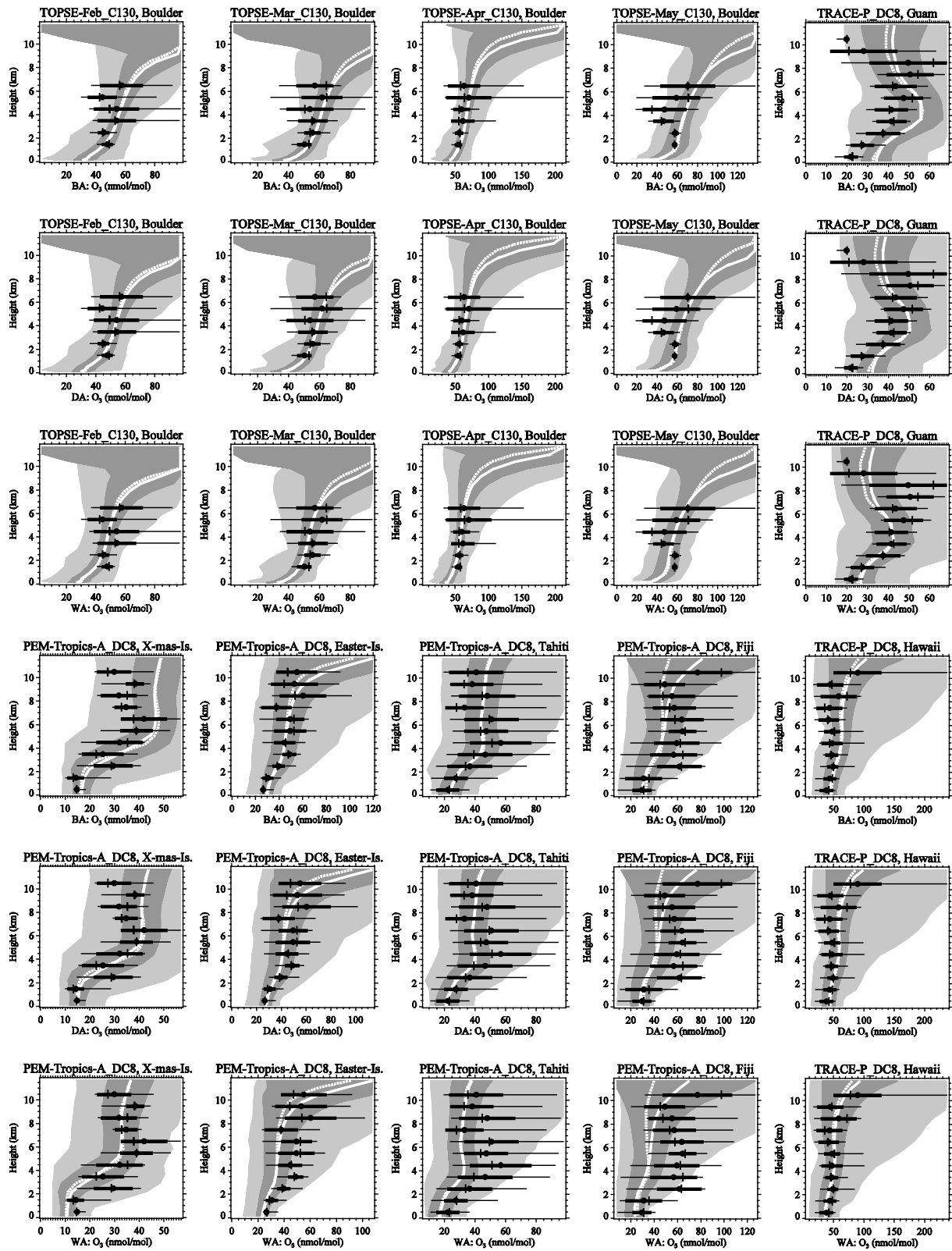


Figure S3b. Continued from Fig. S3a.

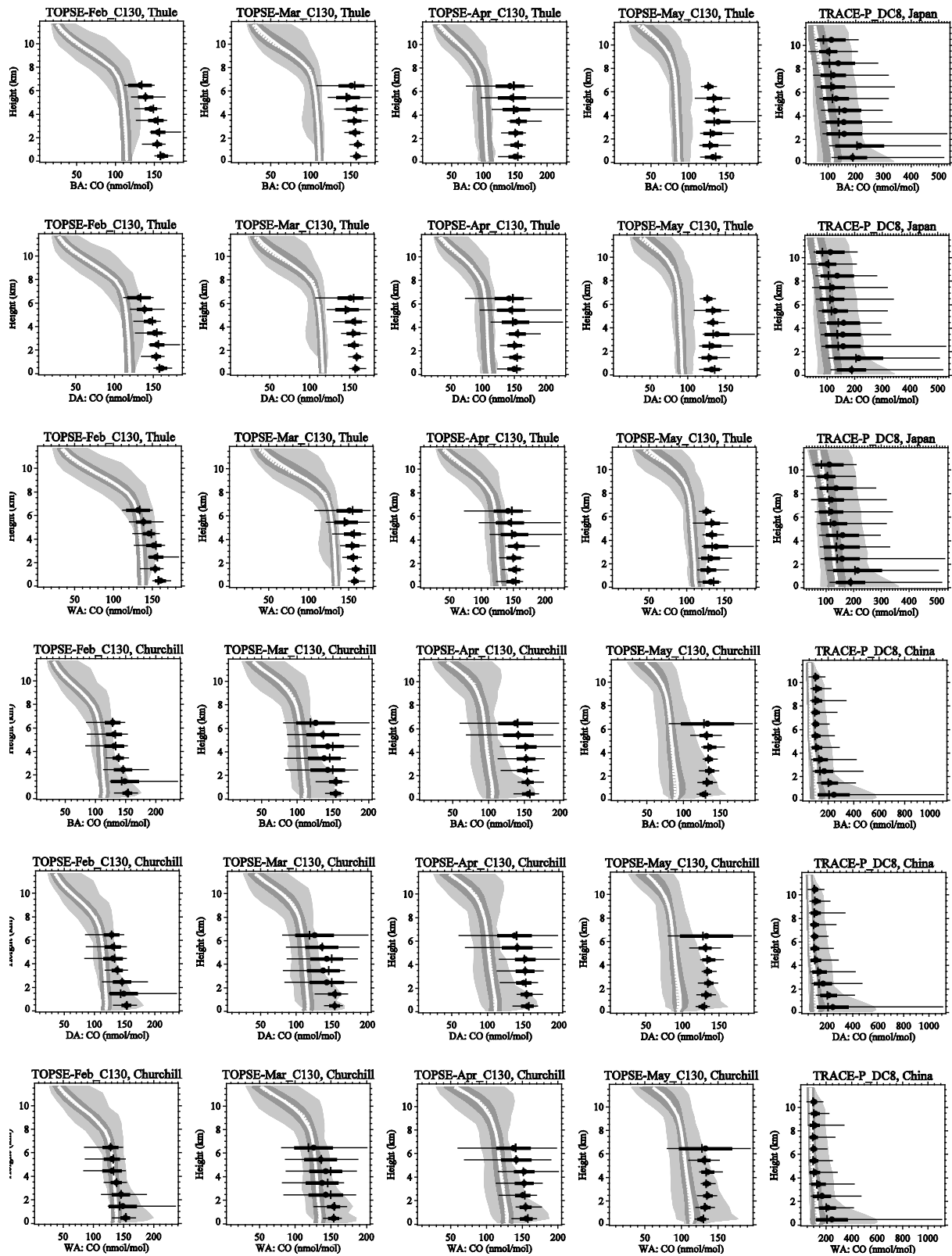


Figure S4a. As Fig. S1a, but for CO.

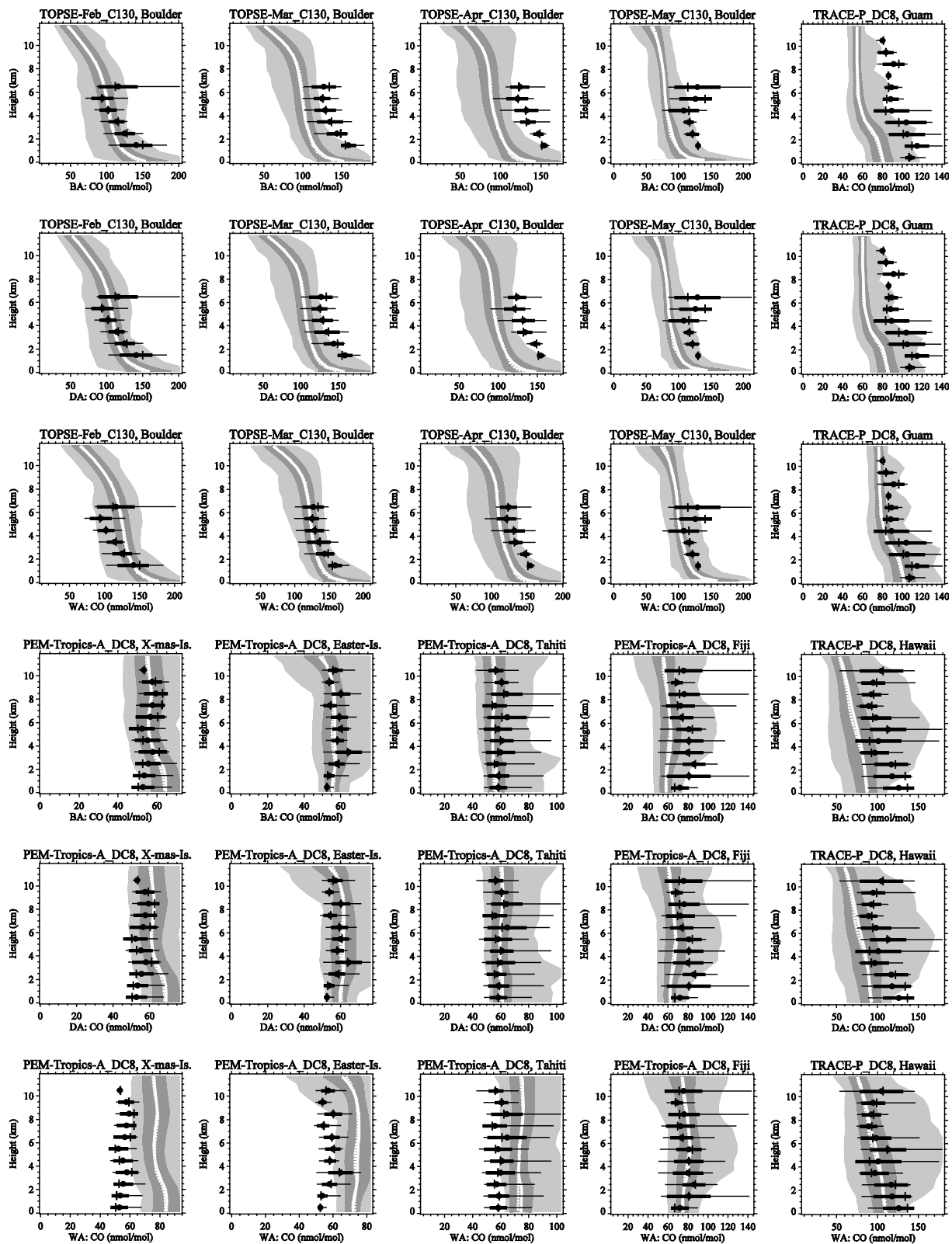


Figure S4b. Continued from Fig. S4a.

2 Additional information on chemical effects

2.1 Branching of $\text{HO}_2 + \text{NO}$

Figure S5 (left) shows the cumulative rate of reactions R1a and R2a. It peaks in the tropics between 10 and 1 hPa, at $0.94 \text{ pmol mol}^{-1} \text{ s}^{-1}$. There is also a smaller local maximum in the tropical UTLS. At most 1 % (R2a) or 5 % (R2b) of the $\text{HO}_2 + \text{NO}$ reaction proceed via the HNO_3 forming channel (Fig. S5, middle and right). NO_x is reused in the catalytic cycle involving R1. Each time a NO_x molecule passes through this cycle, it has a small chance of getting lost via R2. The small branching ratio will consequently be amplified by the cycling. Humidity effects might be slightly underestimated, because all water vapour leading to relative humidity higher than 100 % is immediately transferred into clouds.

A more detailed analysis of the spatial and temporal patterns for the relevant reaction rates (rate coefficients and concentration of educts) would be necessary to fully understand the observed sensitivity patterns. This might be warranted once reaction R2 and its rate coefficient are fully accepted.

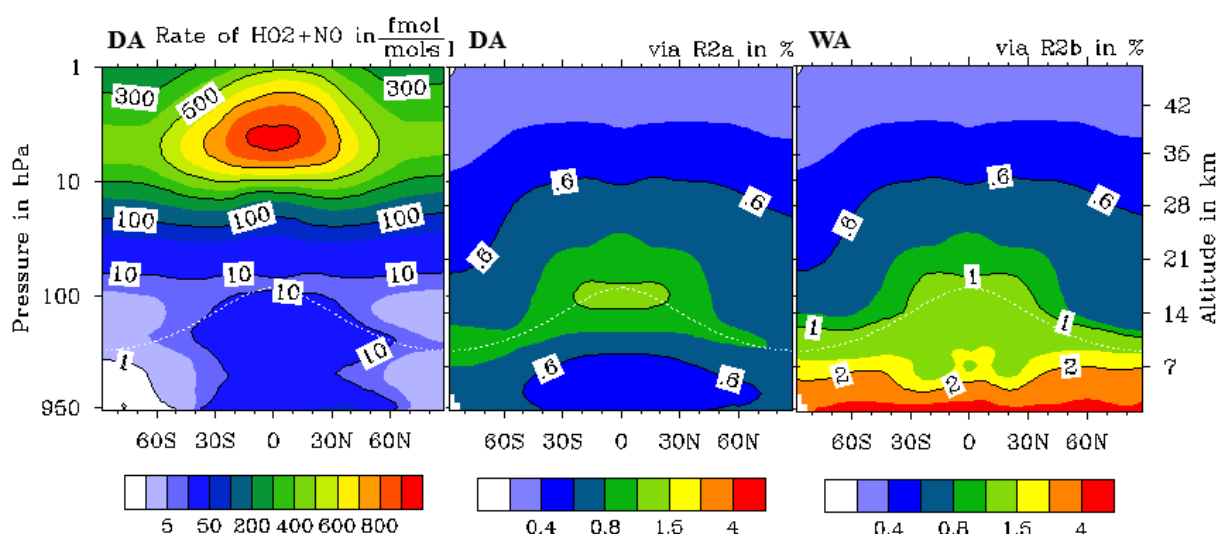


Figure S5. Annual zonal mean reaction rate for $\text{HO}_2 + \text{NO}$ in $\text{fmol mol}^{-1} \text{ s}^{-1}$ (left) in simulation DA. This is similar in the three considered chemical regimes (neglecting feedback via modified educt concentrations). The reaction $\text{HO}_2 + \text{NO}$ proceeds via two channels, with the major channel forming $\text{OH} + \text{NO}_2$, and the minor channel forming HNO_3 . No HNO_3 is formed by the above reaction in simulation BA. The middle picture shows the percentage proceeding via the HNO_3 forming channel assuming a rate coefficient only depending on pressure, temperature (simulation DA). The right picture shows the strength of the minor channel, if the rate coefficient additionally depends on humidity (simulation WA).

2.2 Effects of the HNO₃-forming channel on [O₃], [HO₂] and [NO_y] backgrounds

Butkovskaya et al. (2009) note the difficulty of quantifying the importance of the humidity effect on the reaction rate coefficient of R2 at higher altitudes. Water concentration progressively decreases with altitude, which is partially compensated by the increase of K_{eq} due to decreasing temperature (Eq. 7, Fig. S5). Ozone increases by up to 94 nmol/mol in the tropical stratosphere in DA, but only by 89 nmol/mol in WA (Fig. 1b). According to Eq. 5 humidity should always enhance the effects of R2 (given $\alpha > 0$). Possibly the humidity effect is negligible at this altitude, and enhanced ozone loss from below the zone of no change in zonal mean mixing ratios prints through via atmospheric transport. More aspects of the effects on ozone are discussed in section 3.5 of the main paper.

The [HO_x] = [OH] + [HO₂] response to R2b is dominated by [HO₂], varying from -0.18 to +0.38 pmol/mol in DA and by ± 1.1 pmol/mol in WA, both with respect to BA (Fig. S6, 1st row). HO₂ mixing ratios decrease in WA in the lower troposphere, in the tropics more than at high latitudes. Above is a change of sign in the response, followed by a local [HO₂] increase, reaching more than 50% in the tropical UTLS. Although positive and negative perturbations are higher in WA, the magnitude of the negative perturbation increases more, due to higher humidity at lower altitudes. [HO₂] changes are close to zero for the next 14 km, to rise again locally at 10 hPa. Above is another change of sign and [HO₂] decreases again throughout the uppermost part of the atmosphere. This response pattern is similar for DA, with nearly identical altitudes of zero net response, but lower magnitude in the troposphere. Relative [HO₂] changes are most pronounced in the troposphere, where there is little background [HO₂].

Reactive nitrogen (NO_y) mixing ratios decrease throughout the troposphere, when considering R2, but start to increase above about 20 km (Fig. S6). Relative effects are essentially confined to the troposphere, where zonal annual mean [NO_y] decreases by up to 27 %.

In addition to the overall [NO_x] decrease (Fig. 1b, section 3.5), reaction R2 shifts the NO/NO₂ ratio towards NO throughout the troposphere and UTLS (Fig. S7). The lower NO_x background created by R2 seems to slow down OH- and NO₂-formation by R1, because the OH/HO₂ ratio is also being shifted towards the educt of R2.

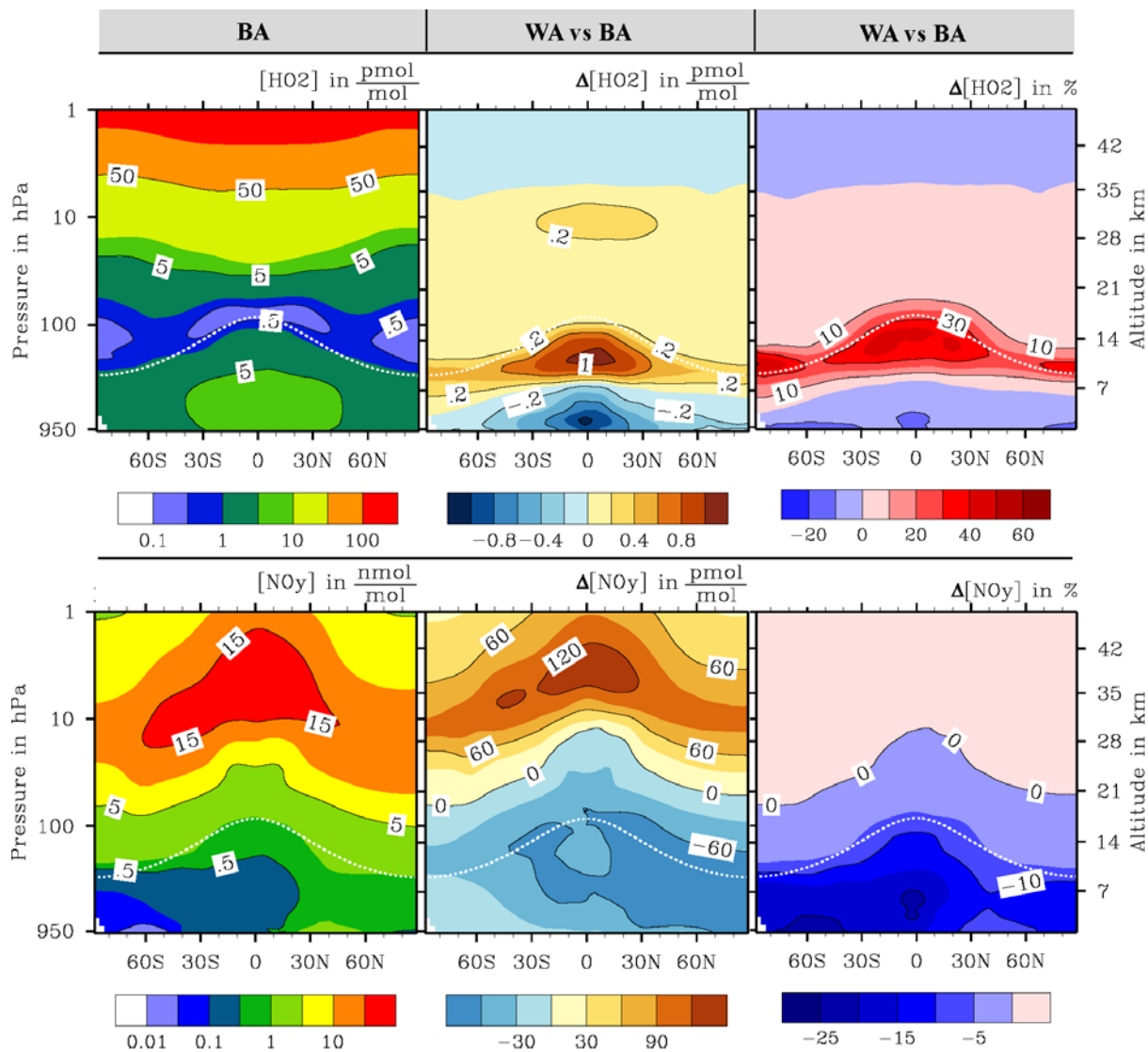


Figure S6. Comparison of $[\text{HO}_2]$ and $[\text{NO}_y]$ in a simulation with the HNO_3 -forming channel to a reference simulation without $\text{HO}_2 + \text{NO} \rightarrow \text{HNO}_3$. Both simulations have identical aviation NO_x emissions. The left column shows annual zonal mean mixing ratios in the reference simulation (BA). The middle and right columns show absolute (WA-BA) and relative deviations when including the HNO_3 -forming channel with a rate coefficient depending on pressure, temperature and humidity (simulation WA). The plots are cut at 1 hPa to zoom into the region of interest, although the uppermost model level is at 0.01 hPa. The white dotted line shows the climatological tropopause according to Eq. 8.

2.3 Chemical effects of aviation $[\text{NO}_x]$ on $[\text{HO}_2]$

The relative $[\text{HO}_2]$ response (not pictured) is nearly identical in ΔB , ΔD and ΔW , reaching -23 %. This corresponds to absolute peak perturbations of -0.43, -0.45 and -0.48 pmol/mol respectively, in the region of maximum aviation NO_x . Below an altitude of about 7 km the $[\text{HO}_2]$ perturbation becomes positive (~ 0.07 pmol/mol in ΔB , ΔD , ΔW). The crossover

between positive and negative response to aviation NO_x occurs at the same altitude as in the background response to R2 (Fig. S6), but with reversed signs. Thus the pattern of $[\text{HO}_2]$ perturbations in Fig. S6 also primarily reflects the inherent response of the photochemical system to $[\text{NO}_x]$ perturbations, which were caused by the introduction of reaction R2.

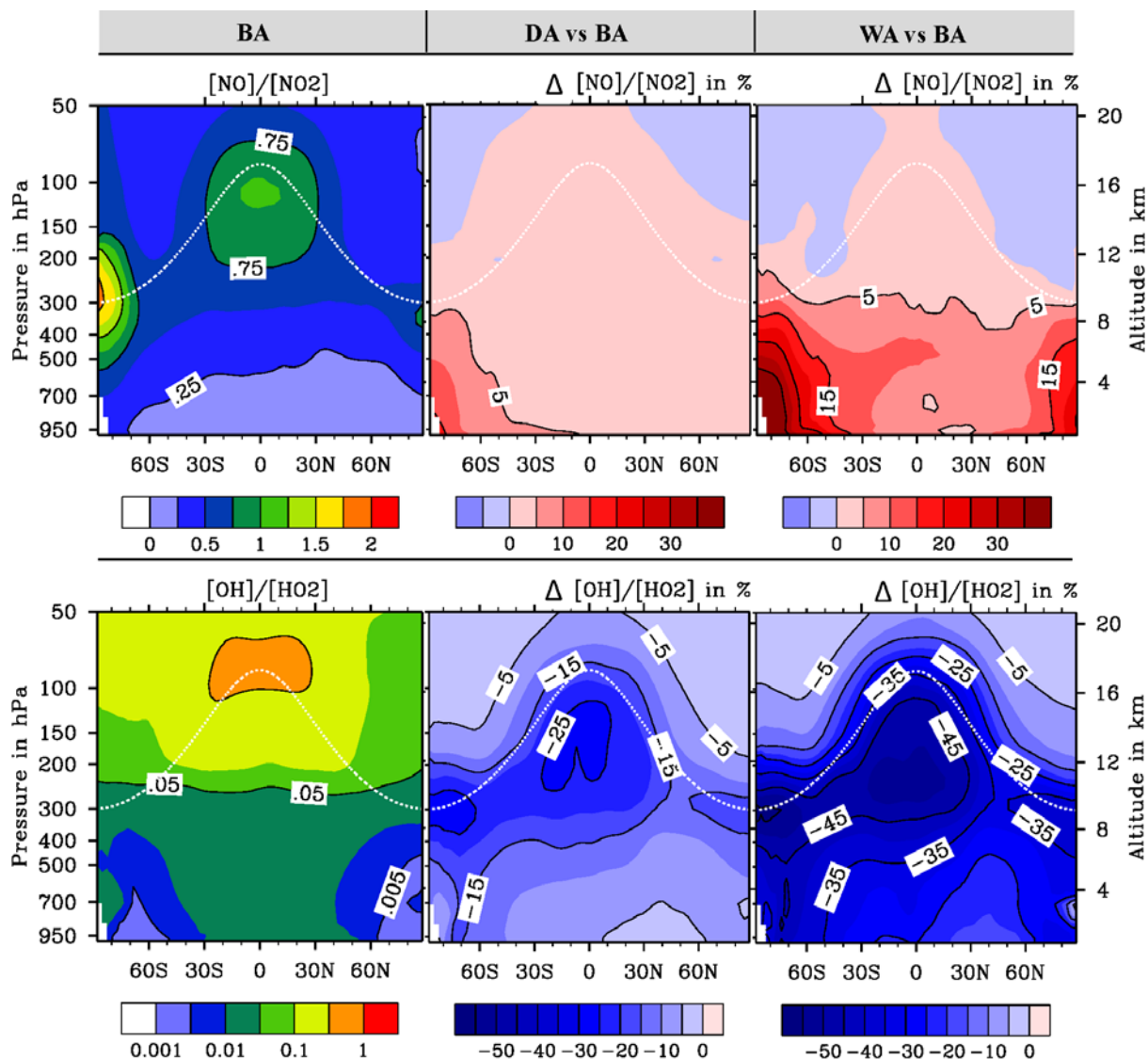


Figure S7. Annual zonal mean ratio of $[\text{NO}]/[\text{NO}_2]$ (top) and $[\text{OH}]/[\text{HO}_2]$ (bottom) in simulations with aviation NO_x . The left column shows the reference case without $\text{HO}_2 + \text{NO} \rightarrow \text{HNO}_3$. Middle and right panels give the relative change of the ratios when considering the HNO_3 -forming channel with rate coefficients $k_2(p, T)$ and, $k_2(p, T, c_{\text{H}_2\text{O}})$, respectively.

2.4 Why is R2 enhancing the effects on [OH] and [O₃]?

For the current study we do not attempt a thorough analysis, and note selected aspects only. Reaction R2 shifts the ratios [OH]/[HO₂] and [NO]/[NO₂] towards [HO₂] and [NO] (Fig. S7). Ambient [HO₂] increases in the UTLS and dominates the [HO_x] response to R2. Background [NO_x] decreases due to R2. More ambient [HO_x] and less [NO_x] may make the coupled catalytic cycles involving those species more sensitive to additional NO_x, which is more of a limiting factor in ΔD and ΔW. Simulations BA, B0, WA and W0 were repeated for short periods of time to diagnose the rates of the main reactions affecting the HO_x and NO_x catalytic cycles. Reactions with HO₂ as educt become less effective above 7 km and more effective below. All other reactions are enhanced by aviation NO_x. The rates of all reactions involving OH, HO₂, NO or NO₂ as an educt are more affected by aviation NO_x in ΔB than in ΔW. Aviation NO_x increases NO_x mixing ratios absolutely more in ΔB than in ΔW, while the relative response is stronger in ΔW. Relative differences between reaction rates in ΔB and ΔW are small, except for the reactions involving OH as an educt. The reactions R4, O₃ + OH → HO₂ and NO₂ + OH → HNO₃ are much more enhanced by aviation NO_x in sensitivity block ΔB than in ΔW. Particularly the relative [OH] response to aviation NO_x is stronger in ΔW, because the main OH loss reactions are weaker in ΔW than in ΔB. Ozone destruction by O₃ + OH → HO₂ is enhanced in response to aviation NO_x in general. The reaction of OH with O₃ is less effective in an atmosphere with R2, due to decreased OH availability. Thus less ozone is destroyed, leading to a stronger ozone signal in sensitivity blocks ΔD and ΔW, compared to sensitivity block ΔB. In turn, more OH is formed by photolysis of the additional ozone, also causing a bigger [OH] perturbation in ΔW. However, the above should be regarded as preliminary ideas that might help to design a thorough analysis.

3 Rate coefficient of $\text{CH}_4 + \text{OH} \rightarrow \text{CH}_3 + \text{OH}$

Here we compare different formulations for the reaction rate coefficient k_{CH_4} of $\text{CH}_4 + \text{OH} \rightarrow \text{CH}_3 + \text{OH}$ (Reaction R4), which has a significant impact on the estimate of methane lifetime. All rate coefficients are given in $\text{cm}^3\text{s}^{-1}\text{molecule}^{-1}$ in the following. The rate coefficients proposed by Gierczak et al. (1997), Atkinson et al. (2003), IUPAC (2007) and Sander et al. (2011) all depend just on temperature. Some studies also provide a value of the rate coefficient at 298 K, which may have a different uncertainty range than formulations with temperature as a parameter would yield at 298 K.

IUPAC (2007) recommends for the temperature (T) range 200 K to 300 K:

$$k_{\text{CH}_4}^{\text{best,min,max}} = 1.85 \cdot 10^{-12} \exp\left(\frac{-1690 \pm 100}{T}\right) \quad (\text{S1})$$

The above formulation has been derived from the more accurate formulation of Gierczak et al. (1997), which is valid for the temperature range 195 K to 296 K:

$$k_{\text{CH}_4}^{\text{best,min,max}} = 1.85 \cdot 10^{-20} \cdot T^{2.82} \exp\left(\frac{-987 \pm 6}{T}\right) \quad (\text{S2})$$

This formulation is also recommended by Atkinson et al. (2003), which is used in this study. The uncertainty at 298 K is estimated to be $\pm 20\%$ (Atkinson, 2003), which is different to the uncertainties given by Gierczak et al. (1997). Sander et al. (2011) recommend

$$k_{\text{CH}_4}^{\text{best}} = 2.45 \cdot 10^{-12} \exp\left(\frac{-1775}{T}\right) \quad (\text{S3a})$$

for 195 K to 300 K, with the uncertainty range

$$k_{\text{CH}_4}^{\text{min,max}} = k_{\text{CH}_4}^{\text{best}} \cdot \left\{ 1.1 \cdot \exp\left| 100 \cdot \left(\frac{1}{T} - \frac{1}{298} \right) \right| \right\}^{\pm 1} \quad (\text{S3b})$$

Uncertainty ranges at 298 K are summarized in Table S2. The temperature dependent formulations (Eq. S1, S2, S3) are plotted in Fig. S8. Their impact on methane lifetime and global mean OH concentration in simulations BA, DA, WA is summarized in Table S3. The recommended temperature dependent rate coefficients ($k_{\text{CH}_4}^{\text{best}}$) of the different studies agree remarkably well (Fig. S8). Thus differences between $\tau_{\text{CH}_4}^{\text{OH}}$ are likely to be small between

different modelling studies that used one of the above formulations for $k_{\text{CH}_4}^{\text{best}}$. The full uncertainty of k_{CH_4} needs to be considered though, when comparing $\tau_{\text{CH}_4}^{\text{OH}}$ from studies that depend on k_{CH_4} to others that do not.

Table S2. Comparison of reaction rate coefficients for $\text{CH}_4 + \text{OH} \rightarrow \text{CH}_3 + \text{OH}$ at 298 K, all in $10^{-15} \text{ cm}^3/\text{s}/\text{molecule}$.

Reference	$k_{\text{CH}_4}^{\text{min}}(298 \text{ K})$	$k_{\text{CH}_4}^{\text{best}}(298 \text{ K})$	$k_{\text{CH}_4}^{\text{max}}(298 \text{ K})$
IUPAC (2007) via Eq. S1	4.56	6.38	8.92
IUPAC (2007) at 298 K	5.32	6.40	7.69
Gierczak et al. (1997) via Eq. S2	6.28	6.40	6.54
Gierczak et al. (1997) at 298 K	6.02	6.40	6.78
Atkinson et al. (2003) via Eq. S2, $\pm 20\%$	5.34	6.40	7.69
Sander et al. (2011) via Eq. S3	5.77	6.35	6.99
Sander et al. (2011) at 298 K	5.73	6.30	6.93

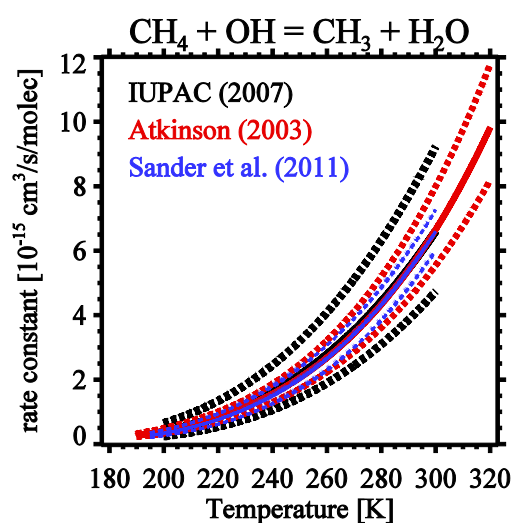


Figure S8. Temperature dependence of the reaction rate coefficient for $\text{CH}_4 + \text{OH} \rightarrow \text{CH}_3 + \text{OH}$ from different studies. Solid curves show the recommended values, dotted lines the corresponding uncertainty ranges.

Table S3. Comparison of methane lifetime and global mean OH concentration for the domain below the climatological tropopause from Eq. 8, and for the domain below 100 hPa (in parentheses). $\tau_{\text{CH}_4}^{\text{OH}}$ is given in years, $\langle c_{\text{OH}} \rangle$ in 10^6 cm^{-3} . Minimum (min), best and maximum (max) values reflect the uncertainty ranges of the rate coefficient for $\text{CH}_4 + \text{OH} \rightarrow \text{CH}_3 + \text{OH}$, as given by Eq. S1, S2 and S3. Note that the uncertainty given by Eq. S3b is a factor. It occurs in numerator and denominator of the weighting and thus has no effect on $\langle c_{\text{OH}}^k \rangle$.

	BA			DA			WA		
	min	best	max	min	best	max	min	best	max
$\tau_{\text{CH}_4}^{\text{OH}}$ (IUPAC, 2007)	(5.5)	(7.9)	(11.4)	(6.1)	(8.7)	(12.6)	(8.2)	(11.8)	(17.0)
	5.2	7.5	10.8	5.7	8.3	11.9	7.8	11.2	16.1
$\tau_{\text{CH}_4}^{\text{OH}}$ (Atkinson, 2003)	(6.7)	(8.1)	(9.7)	(7.4)	(8.9)	(10.7)	(10.0)	(12.0)	(14.4)
	6.3	7.6	9.1	7.0	8.4	10.1	9.5	11.4	13.7
$\tau_{\text{CH}_4}^{\text{OH}}$ (Sander et al., 2011)	(7.2)	(8.2)	(9.2)	(8.0)	(9.0)	(10.2)	(10.7)	(12.2)	(13.8)
	6.8	7.7	8.7	7.5	8.5	9.6	10.2	11.5	13.0
$\langle c_{\text{OH}}^{\text{mass}} \rangle$		(1.22)			(1.09)			(0.823)	
		1.27			1.13			0.850	
$\langle c_{\text{OH}}^k \rangle$ (IUPAC, 2007)	(1.39)	(1.40)	(1.41)	(1.26)	(1.27)	(1.28)	(0.935)	(0.942)	(0.949)
	1.41	1.41	1.42	1.27	1.28	1.29	0.943	0.950	0.956
$\langle c_{\text{OH}}^k \rangle$ (Atkinson, 2003)	(1.40)	(1.40)	(1.40)	(1.27)	(1.27)	(1.27)	(0.945)	(0.945)	(0.945)
	1.42	1.42	1.42	1.29	1.29	1.29	0.953	0.953	0.953
$\langle c_{\text{OH}}^k \rangle$ (Sander et al., 2011)	(1.40)	(1.41)	(1.42)	(1.27)	(1.28)	(1.29)	(0.941)	(0.948)	(0.955)
	1.41	1.42	1.43	1.28	1.29	1.30	0.949	0.955	0.961

References

- Atkinson, R.: Kinetics of the gas-phase reactions of OH radicals with alkanes and cycloalkanes, *Atmos. Chem. Phys.*, 3, 2233–2307, 2003.
- Atkinson, R., Baulch, D. L., Cox, R. A., Crowley, J. N., Hampson, R. F., Hynes, R. G., Jenkin, M. E., Rossi, M. J., and Troe, J.: Evaluated kinetic and photochemical data for atmospheric chemistry: Volume I - gas phase reactions of O_x, HO_x, NO_x and SO_x species, *Atmos. Chem. Phys.*, 4, 1461-1738, doi:10.5194/acp-4-1461-2004, 2004.
- Emmons, L. K., Hauglustaine, D. A., Müller, J.-F., Carroll, M. A., Brasseur, G. P., Brunner, D., Staehelin, J., Thouret, V., and Marenco, A.: Data composites of airborne observation of tropospheric ozone and its precursor, *J. Geophys. Res.*, 105, 20 497–20 538, 2000. Data downloaded from http://acd.ucar.edu/~emmons/DATACOMP/camp_table.htm.
- Gierczak, T., Talukdar, R. K., Herndon, S. C., Vaghjiani, G. L., and Ravinshankara, A. R.: Rate Coefficients for the Reactions of Hydroxyl Radicals with Methane and Deuterated Methanes, *J. Phys. Chem. A*, 101, 3125-3134, 1997.
- Holmes, C. D., Tang, Q., and Prather, M. J.: Uncertainties in climate assessment for the case of aviation NO_x, *P. Natl. Acad. Sci. USA*, 108, 10997-11002, www.pnas.org/cgi/doi/10.1073/pnas.1101458108, 2011.
- IUPAC: IUPAC Subcommittee on Gas Kinetic Data Evaluation – Data Sheet HO_x_VOC1, <http://www.iupackinetic.ch.cam.ac.uk/index.html>, updated 12. 12. 2007, (see also Atkinson et al., 2004), 2007.
- Jöckel, P., Kerkweg, A., Pozzer, A., Sander, R., Tost, H., Riede, H., Baumgaertner, A., Gromov, S., and Kern, B.: Development cycle 2 of the Modular Earth Submodel System (MESSy2), *Geosci. Model Dev.*, 3, 717-752, doi:10.5194/gmd-3-717-2010, 2010.
- Keene, W. C., Sander, R., Pszenny, A. A. P., Vogt, R., Crutzen, P. J., and Galloway, J. N.: Aerosol pH in the marine boundary layer: A review and model evaluation, *J. Aerosol Sci.*, 29, 339–356, doi:10.1016/S0021-8502(97)10011-8, 1998.
- Sander, S. P., Barker, J. R., Golden, D. M., Kurylo, M. J., and Wine, P. H.: Chemical Kinetics and Photochemical Data for Use in Atmospheric Studies, Evaluation Number 17, JPL Publication 10-6, Jet Propulsion Laboratory, Pasadena, CA, 2011.